

A traveling wave of lateral movement coordinates both turning and forward walking in the ferret

Neri Kafkafi, Ilan Golani

Department of Zoology, George S. Wise Faculty of Life Sciences, Tel-Aviv University, Tel-Aviv, Israel

Received: 26 August 1997 / Accepted in revised form: 12 March 1998

Abstract. Relative phase was recently suggested as a key variable for the dynamical modeling of coordination in both quadruped locomotion and undulation swimming in fish. Relative phase analysis has not yet been applied, however, to the behavior of intact, freely moving animals, but only to simplified situations involving restrained animals and humans. In order to investigate relative phase under free movement conditions, we filmed free locomotion of ferrets (*Mustella putorius*) from below (through a glass floor) and measured the lateral bending along the head, torso, and tail, and the location of the four paws. We introduced an algorithm which extracts the phase (and thus also the relative phase) even when the movements were neither periodic nor symmetric. Our results show that relative phases between segments have preferred values, which are relatively independent of the amplitude, duration, and asymmetry of the movement. In particular, both walking and turning can be explained as modulations of a single pattern: a cephalo-caudal, traveling wave of lateral movement with a wavelength of approximately one length of the body. The relative phase between movements of adjacent segments is similar when the body is in S shape (i.e., when walking forward), or C shape (i.e., when turning). The movements of the paws in the horizontal plane can also be considered as part of this traveling wave. Our findings suggest that the concept of traveling waves of lateral bending, as found in the locomotion of undulating fish, can be generalized in two ways: (i) by considering the axis around which the movement is centered, it applies not only to forward locomotion, but also to turning; (ii) by incorporating the position of the paws, it applies also to the movement of quadrupeds. Our findings suggest that the relative phase, once it is generalized to asymmetric and quasi-periodic movement, is suitable for modeling coordination patterns under free movement conditions.

1 Introduction

In recent years, patterns of interlimb coordination, particularly the gaits of quadruped locomotion, have been modeled as dynamical systems of coupled oscillators. In these models, the relative phase between the movements of the limbs was shown to be a good collective variable, i.e., there is a particular value of it (e.g., half a cycle between the forelegs during trot) which is stabilized and thus can be considered a point attractor. Relative phase models are useful because they explain additional phenomena in quadruped locomotion, such as sudden bifurcations of the relative phase from one stable value to another when the gait is changed (for review, see Schoner et al. 1990; Turvey 1990; Collins and Stewart 1993; Kelso 1995).

Relative phase (ϕ_{rel}) is also considered as a key variable in the undulation pattern of swimming in eel-like fish. The undulation is coordinated by a wave of lateral bending that travels from head to tail. This traveling wave has a wavelength of approximately one length of the body (i.e., the body assumes an S-shape while swimming because one wave is present at all times). This wavelength is kept constant during a wide range of undulation frequencies (Grillner and Kashin 1976). It follows that ϕ_{rel} (or the “phase lag”) between succeeding segments of the body is stabilized to a value of some small fraction of a cycle, so that the sum of the ϕ_{rel} 's along all the segments of the body equals (approximately) one cycle. The neural mechanism in the spinal cord that underlies this pattern has been intensively investigated in the lamprey (*Petromyzon* sp.), which is currently the most important experimental model for the structure and function of the spinal cord. Models for explaining the traveling wave pattern are now well-developed, both on the neural level (Grillner et al. 1995; Jung et al. 1996) and on the more abstract level of coordination dynamics (Kopell 1988; Rand et al. 1988; Yuasa and Ito 1990).

ϕ_{rel} is thus perceived as a key variable of locomotor patterns in both quadrupeds and fish. Nevertheless,

Correspondence to: N. Kafkafi
 (e-mail: oferner1@ccsg.tau.ac.il, ilan99@ccsg.tau.ac.il,
 Tel.: +972-3-6407350, Fax: +972-3-6409403)

when trying to apply ϕ_{rel} to understand locomotor patterns in free (unrestrained) vertebrate behavior, some methodological difficulties arise. Most of the existing experiments and models employ a simplified situation in which the animal locomotes at a fixed (or gradually changing) speed, so that the resulting pattern is strictly periodic. Most of them also restrain (or assume) the animal to locomote on a straight line, which means that the resulting pattern is left-right symmetric (but see Ekeberg 1993). Owing to these simplifications, the movement of each limb/segment can be adequately described by a single variable: its phase. The phase can be measured by only one or two particular events in the cycle namely the peaks of the limb/segment displacement. Between these peaks, the phase is only assumed by interpolation. The problem is how to measure phase in real life situations, in which movement is often asymmetric and aperiodic.

A graphical representation of this problem is shown in Fig. 1. Column A represents the simplified situation: the movement of each segment of the body (top) is assumed to be periodic and left/right symmetric. The time-series of the angle of one segment relative to the other (middle) is thus centered on zero (=straight). The period T , measured as the time lapse between two peaks, and the amplitude A are constant (locally at least) and thus can be ignored. The phase is defined as $0 = 1$ at

the peaks, and is computed by interpolation for any other instant of the cycle as the proportion of T .

The phase-plane (bottom) plots the first derivative of the angle (i.e., the angular velocity) vs the angle itself. In this representation, every cycle is plotted as a loop (a circle if the time-series is sinusoid). If the movement is symmetrical, the loop is centered at the origin of axes, and the phase Φ at any point can be represented by the angle between a line from this point to the origin of axes, and the x -axis. After computing the phase for each movement, ϕ_{rel} is the phase difference between two concurrent movements (e.g., Schoner et al. 1990; Kelso 1995).

While the assumptions of periodicity and symmetry considerably simplify the treatment of ϕ_{rel} , they also make it impossible to apply it directly to free locomotor behavior. When a fish or a mammal turns, for example, each segment of the body bends (relative to the more posterior segment) to the side of the turn and then straightens again; in this case (column B, Fig. 1) the time lapse between peaks cannot be used, and the movement is not symmetric. This case, however, can be thought of as a single cycle of a periodic movement (Fig. 1B, middle, dashed line) centered around angle C ("center of oscillation"), which in this case is different from zero. In the phase-plane (Fig. 1B, bottom), this situation is plotted as a loop which is off-centered to one side by C , and the phase Φ at any moment is the

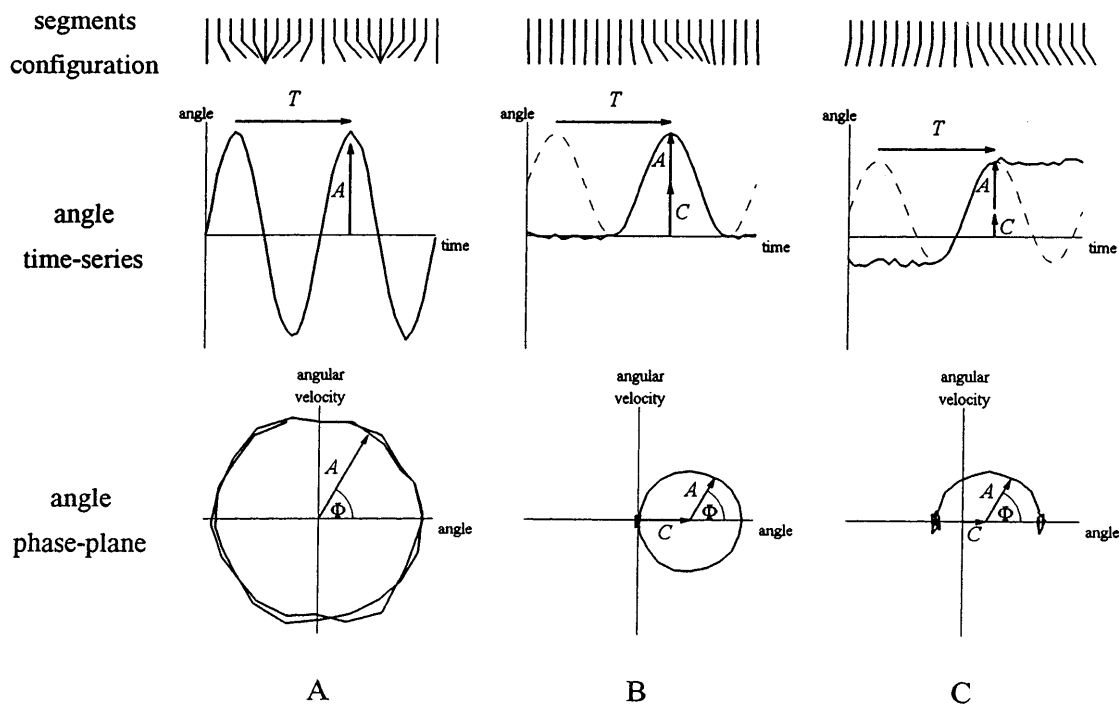


Fig. 1. The conventional (column A) and generalized (columns B, C) concepts of phase in a time series. *Top row* shows how the angle between two segments of the body changes with time (denoted by the *time axis* of the corresponding graph below it, in the *second row*). *Middle row* shows the angle time-series. *Third row* shows the angle phase-plane (angle vs its first derivative or angular velocity). *Column A* shows the common method for measuring the phase in a periodic, symmetric time-series: The period T is the time lapse between peaks, and the phase of every instant during that time is measured in fractions of T (analogous to the angle Φ in the phase plane). *Column B* represents a situation of bending and straightening, where the time-series is neither symmetric nor periodic. This situation can be modeled as a local periodic movement (dashed line), centered on a "center of oscillation" C . The justification for this modeling is clearer in the phase-plane (bottom). A discrete movement (column C) is modeled in the same way as half a cycle. See text for further explanation

angle created with the loop's center (C , 0) on the horizontal axis.

Finally, many of the movements in free behavior are not periodic at all, but discrete (Fig. 1C, top). Such movements can be referred to as half a cycle of a periodic movement (Fig. 1C, middle, dashed line) and are plotted in the phase-plane as half a loop, starting and ending on the horizontal axis, in which Φ at every moment can still be computed as in the previous case. The simplified situation in Fig. 1A can thus be conceived of as a particular case of the more general concept of phase, in which C , A , and T are not necessarily constant and therefore cannot be neglected.

In this study, we tested the hypothesis that coordination patterns of free behavior are also characterized by the stability of ϕ_{rel} . To test this hypothesis, we developed an algorithm, based on the concept outlined above, to compute phase during free movement. The algorithm takes as data the time series of any variable (e.g., the angle between two segments) and models every instant of it as part of a local periodic movement, as suggested by the dashed lines in Fig. 1B and C. The value of the variable at this specific instant can thus be separated into four components: The parameters Φ , C , A , and T of that periodic movement. The algorithm (hence referred to as the Φ CAT algorithm) can compute these four components at any instant of the movement. ϕ_{rel} of any two concurrent movement is, as mentioned before, their phase difference.

As an experimental model for investigating ϕ_{rel} during free movement, we used ferrets (*Mustella putorius*) filmed from below through a glass floor. Figure 2 shows six frames from a free movement sequence of a ferret. Ferrets display a rich repertoire of motor patterns in-

volving a considerable lateral component: lateral bending while walking, turning in place or while walking, and scanning movement with head and neck. We will examine the hypothesis that this repertoire is executed with a preferred ϕ_{rel} , which is relatively independent of the other components C , A , and T of the movement.

If ϕ_{rel} is indeed stabilized to a specific value or values, it will be of interest to determine these values. As mentioned before, the traveling wave pattern of undulation swimming in fish is created by a slight lag of the more caudal segment relative to the more anterior (ϕ_{rel} is a small fraction of a cycle, but different from zero). In tetrapoda (quadruped vertebrates), in contrast, lateral movement during walking is commonly thought to involve a standing wave. In a standing wave, there is no lag of the caudal segment ($\phi_{\text{rel}} = 0$ cycles), except over particular locations along the body (the "nodes" of the wave) in which ϕ_{rel} is changed by half a cycle. The notion that walking in tetrapoda involves a standing wave is based on studies in some urodela (salamanders, newts, etc.) and lizards (Cohen 1988), but to our knowledge has never been examined in mammals. Our experimental setup made it possible to examine the type of wave characterizing the ferret. We also argue that our novel method for evaluating the wave type, based on direct measurement of the phase and of ϕ_{rel} , is more reliable than the usual method, which is based on the lateral displacement of points on the body.

The Φ CAT algorithm also allowed us to test the hypothesis that turning and forward walking are modulations of the same pattern in vertebrates. When a vertebrate turns, it usually starts with lateral bending of the head to the side of the turn. The other segments of the body then join in a cephalocaudal order. Concomi-

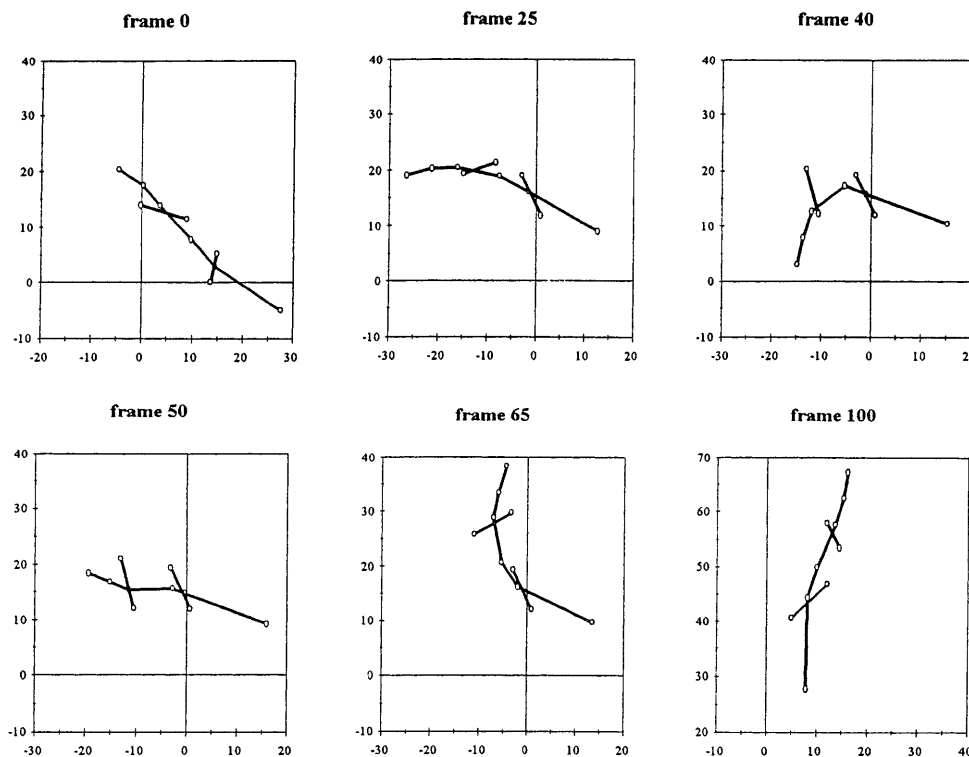


Fig. 2. Six selected frames from a 120-frame (4.80-s) sequence of free movement of a ferret. The movement was filmed from below and measured by using 10 points on the animal's body (*open circles*), which define 7 "segments": body segments (from *left to right* in, e.g., frame 25): Head, Neck, Chest, Pelvis, and Tail; and Forelegs and Hindlegs, which form two "virtual" segments, connecting the forepaws and hindpaws, respectively. Coordinate frame of the observation platform is the same in all frames, given in centimeters from a specific origin point common to all. The animal walked forward, stopped, made half a turn to the left, and then turned and walked to the right

tantly, the head straightens again, and straightening also travels cephalocaudally along the body (Gray 1933; Golani 1976; Jayne and Lauder 1993; Ullen et al. 1993). In this paper we test the hypothesis that in ferrets this bending and straightening travels along the body at a fixed phase lag, similar to that of forward walking. We also examine whether this is true for the lamprey, by reinterpreting data from the literature. If true, this could mean that a turn is simply an asymmetric forward locomotion, and that it can be executed by modulating only one parameter, the “center of oscillation” C of the ΦCAT algorithm.

During presentation and discussion of the results, we stress the point that, as long as the components C , A , and T are taken into consideration, treating coordination patterns of free behavior in terms of ϕ_{rel} between segments is useful even when the movement is not strictly periodic and regular.

2 Methods

2.1 Experimental animals

Ferrets had two advantages for the present study: (i) their elongated body, especially in females, allows for a more accurate measurement of horizontal bending; (ii) they exhibit a high level of activity in an unfamiliar area, thus providing sufficient data for analysis. Four adult females weighing 500–800 g were used, all of the same strain, bred at the animal facilities of the Hebrew University.

2.2 Filming

Filming was done from below through a glass floor. This method has been used in previous work with laboratory rats (e.g., Eilam and Golani 1988; Kafkafi et al. 1996) and has been found to facilitate an accurate evaluation of the horizontal directions of head, trunk and tail, and of the direction and timing of stepping in all four legs. The observation platform was a 1.8×1.8 m flat glass plate, placed horizontally about 2 m above the ground. A large mirror placed under the glass floor, tilted at 45° to it, allowed videotaping of a bottom view of the animals. The lower face of the glass was covered with a square grid of 10 mm colored stickers, 16 cm apart, which provided a reference coordinate frame for measurement (see Sects. 2.3 and 2.4). The center of the platform contained a cross-shaped plastic partition, 40 cm high and 100 cm long from edge to edge. This partition prevented the animal from seeing the entire platform at once, thus encouraging it to explore continuously and not spend all of its time at the edges.

Each animal was marked along the midline of the ventral side with four colored 10 mm stickers: (i) below the posterior edge of the mandibula; (ii) on the anterior edge of the sternum; (iii) on the posterior edge of the sternum; (iv) 10 mm in front of the pubis. The four paws were painted with fast-drying, non-toxic correction fluid. Each of the animals was placed on the observation platform and filmed for 20 min. All of the animals were naive and tested once. The platform was washed with detergent before each session.

All animals performed varied and intensive locomotor behavior throughout most of the 20-min filming period. Activity always started immediately after introducing the animal into the set-up, and no fear reactions due to the glass transparency were observed.

Filming was performed with a Super VHS video camera, using a 1/250-s shutter speed for accurate recording of fast movements. In order to obtain as large an image as possible, we zoomed in on

the animal with the tripod-mounted camera, and followed it as it moved around on the platform. The video films were time-coded (hour, minute, second, and frame).

2.3 Data acquisition

Sequences for measurement were selected from the videotapes by first choosing a randomly sampled frame out of the 20-min film and then selecting the next nearest sequence which fitted all the following criteria: (i) the animal had been moving for at least 2 s; (ii) periods of immobility within the sequence lasted for no more than 0.75 s; (iii) there were no large vertical and rotational (“log-rolling”) movements in the sequence; (iv) the markers were not hidden for most of the time (see below). The total number of sequences measured per animal was 14, 12, 15, and 16, and the total duration per animal was 61, 48, 60, and 61 s. Since free behavior is typically intermittent, most sequences lasted for 3–7 s.

Measurement was performed with a super-VHS videotape at a rate of 25 frame/s. Initially, a rate of 50 frame/s was also used, but it was found that the higher time resolution was not needed. Data acquisition was performed with an interactive (automatic/manual) tracking program developed by us, which recognizes targets by correlating current to previous pixel values of the same target (correlation tracking). The screen coordinates of 10 points were measured by the tracking program in each frame: the four stickers mentioned in the previous section, the tip of the snout, the tip of the tail, and the centers of the four paws. In addition, in each frame the tracking system measured three points, arranged in a straight angle, of the grid marked on the observation platform. These points were used as a reference frame for measurement (see also Sect. 2.4). Depending on the observation conditions, tracking was performed either automatically or manually.

If the target was hidden for one or two frames, its coordinates in these frames were computed by linear interpolation. If the target was hidden for more than two frames, its location was determined manually by the user, taking into account the visible body parts and the location of the target in nearby frames. Sequences in which at least 1 of the 13 points was hidden for more than 10% of the time were excluded from measurement.

The average accuracy of measurement was evaluated by measuring the same sequence by different users, by the same user at different times, or by automatic vs manual tracking. This amounted to about ± 3 pixels in screen coordinates, which corresponds to about ± 0.4 cm in space coordinates. Thus, the accuracy of measuring the angle between segments (see Fig. 2) was $\pm 4^\circ$ to $\pm 8^\circ$, depending on the segment’s length. The head was the shortest segment measured (about 5 cm long), and the range of its movement was also the smallest ($\pm 45^\circ$), which means that the precision of measuring the head angle was the lowest.

2.4 Data processing methods

In order to compensate for the movement of the camera, we first computed the coordinates of the measured points in the absolute frame of reference. This was done by a coordinate transformation, using the three grid points measured off the observation platform (see Sects. 2.2 and 2.3) as reference. From the absolute coordinates, we computed the angles between the segments, the velocities, the segment absolute directions, etc. An animation of the movement was also computed from the data (six frames sampled from such a video clip are presented in Fig. 2).

It is interesting to note that although our animated ferret is quite schematic, being composed of only 10 points, it appears lively and natural once it is moving. This suggests that 10 two-dimensional coordinates (i.e., 20 degrees of freedom) would be sufficient for formulating the coordination patterns which are recognized subjectively by “experienced observers” (Beer 1980; and see discussion in Sect. 4.4).

3 Results

3.1 General properties of free locomotor behavior of ferrets

The observed behavior was varied and complex even after excluding movements with considerable vertical or rotational components. The behavior included scanning movements with the head and neck, tight and wide turns, forward walking, starts and stops, and complex simultaneous combinations of the above. A diagonal gait was not always maintained, mainly due to turning. In particular, hindleg stepping was omitted during tight turns. When the animal started a turn from a standing position, it stepped first either with the inside or outside foreleg, with no apparent correlation to any property of the turn. In summary, free behavior cannot be decomposed in a trivial way into stereotyped components such as “forward walking” and “turning”.

3.2 Computation of ϕ_{rel}

To compute ϕ_{rel} , we divided the ferret into seven segments (Fig. 2): Five segments of the body – head, neck, chest, pelvis, and tail (seen, for example, from the top downward in the last frame in Fig. 2) – and the forelegs and hindlegs, which are considered as two “virtual” segments created by connecting the forepaws together and the hindpaws together (seen as crossing the trunk in Fig. 2); h , n , c , and p denote the angles between

head and neck, between neck and chest, between chest and pelvis, and between pelvis and tail, respectively; ff denotes the angles between forelegs and chest, and hh denotes the angles between hindlegs and pelvis. The angles h , n , c , and p between the segments of the trunk are defined as zero when the two segments are in line, while the angles ff and hh of the legs are defined as zero when they are orthogonal to the chest or pelvis. Thus, when the ferret stands in a natural and symmetrical position, all angles equal zero.

Figure 3 (top) shows an example of a time series of one angle from the data (represented by the dots), as measured 25 times (frames)/s. We used the Φ CAT algorithm in order to compute the phase at any frame n , by modeling it as part of a local periodic movement, and computing the coefficients (including the phase) of this periodic movement (see dashed lines in Fig. 1B, C). For this, the Φ CAT algorithm considered the moving “time window” centered around frame n and $2k + 1$ wide: $[n-k, n-k+1, \dots, n, n+1, \dots, n+k]$, and fitted the data within this window with a cosine curve (see examples in Fig. 4). The fit was done by least-square optimizing of C , A , T , and Φ , the four parameters in the cosine equation:

$$y(i) = C + A \times \cos\left(\frac{2\pi}{T}i - 2\pi\Phi\right) \quad (1)$$

where:

i is the index of the frames in the time window, moving from $-k$ to $+k$ and equaling 0 at the considered frame n ;

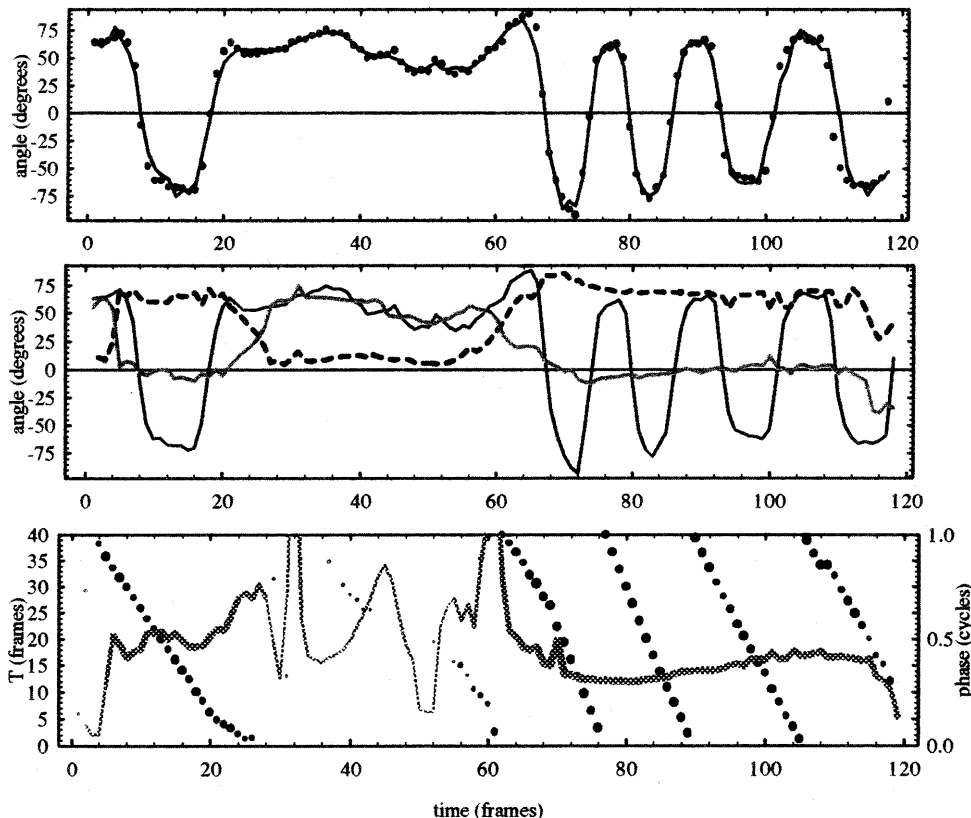


Fig. 3. Decomposition of an angle time-series into amplitude A , center of oscillation C , period T , and phase Φ . The *top* graph shows an original time-series of the foreleg angle (*black dots*). In the *middle* graph the data (*bold line*) are shown together with the computed center of oscillation C (*gray line*) and amplitude A (*dashed line*), both measured in degrees. The *bottom* graph shows the computed period T (*line*, measured in frames) and phase (*black dots*, measured in cycles). In the bottom graph, the thickness of the line (in the case of T) and the dot size (in the case of Φ) represent the amplitude. This mode of representation highlights the fact that both Φ and T have no meaning when the amplitude approaches zero (i.e., immobility is represented by an almost invisible line or dots). From the computed Φ , A , C , and T , an estimation of the original angle can be computed. The estimated angle is shown in the top graph (*line*) together with the original data (*dots*).

$y(i)$ is the estimated value of the angle at frame i (which is to fit the data);

C is the (local) center of oscillation, measured in degrees, i.e., the value around which the data oscillate in the time window considered. In graphical terms, it is the vertical displacement of the cosine curve in Fig. 4;

A is the (local) amplitude of oscillation, measured in degrees, around the center C (i.e., the vertical distance of the peaks of the cosine curve from C);

T is the local period, measured in frames, of one cycle in the time window (horizontal length of one cycle of the cosine curve);

Φ is the phase, measured in units (from 0 to 1) of the period T (i.e., the horizontal displacement of the cosine curve, as a fraction of one cycle).

Note that (1) is the standard equation for pure harmonic (i.e., sinusoid) motion. Six examples of time windows, with the best-fit curves generated by the Φ CAT algorithm, are shown in Fig. 4. The data point at the center of each window ($i = 0$) is the frame n that has been decomposed by the algorithm into its four components.

As the examples in Fig. 4 show, the shape of the angle time series was not strictly sinusoidal. The time series of the two angles of the legs, ff and hh , were more “square” in shape (see Fig. 4B, D), because when both forelegs (or both hindlegs) were on the ground, the angle change was only due to the movement of the chest (or of the pelvis), a change which is relatively small in comparison to the change when a leg is off the ground. The time series of the body angles were more “saw-like”, and occasionally had a small deceleration near the middle of the movement (Fig. 4A, C). The reason for this is not clear, but could be due to a vertical component of the movement. In order to correct our model for these “deformations” of the curve’s shape, we used a deformation function D with a “deformation parameter” b :

$$D(x, b) = x + b \sin(\pi x); \quad 0 \leq x \leq 1 \quad (2)$$

When this function is applied to a variable x that oscillates sinusoidally, it yields a more “square” oscillation with b slightly larger than 0 and a more “saw-like” oscillation with b slightly smaller than 0. When D is

applied to the cosine term in (1), we obtain its “deformed” version:

$$y(i) = C + A \times D \left[\cos \left(\frac{2\pi}{T} i - 2\pi\Phi \right), b \right] \quad (3)$$

We therefore actually used (3), which fits the data with a saw-like oscillation (for $b < 0$) or square oscillation (for $b > 0$) rather than a sinusoidal oscillation. We used fixed values of $b = 0.2$ for leg angles and $b = -0.25$ for body angles, since these values seemed to yield a good fit for the data (see again the data points and the fitted curves in the examples in Fig. 4). It is important to note that the results of our analysis of ϕ_{rel} (Sect. 3.3) were similar using either (1) or (3). In fact, they did not change much even when using the simple statistical methods we used to generate starting values for the fitting algorithm (see below and in the Appendix). Using an algorithm that can handle non-harmonic movement might, however, be of significance with more complex methods of analysis.

We used a least-squares fit, weighted more in the middle of the time window than on its edges (Fig. 3 shows that the curves usually fit better in the middle of the window). For a weight function, we used a Gaussian with a standard deviation of three frames. Thus, a point at a distance of, e.g., 9 frames (= 3 standard deviations) from the considered point contributed almost nothing to the shape of the curve. The algorithm was implemented with the function “NonlinearFit” in the statistics package of Mathematica software (Wolfram Research Inc. 1993). Some technical considerations of implementing the algorithm are discussed in the Appendix.

The angle at any frame of the time series is thus decomposed into values of C , A , T , and Φ . Figure 3 (middle and bottom) shows an example of the computed C , A , T , and Φ for one time-series. C and A are measured in degrees, T is measured in frames (1 frame = 1/25 s), and Φ is measured in fractions of one cycle. The algorithm gives Φ as moving from -0.5 to $+0.5$ (in terms of radians, from $-\pi$ to π ; in terms of degrees, from -180° to 180°). It is convenient to consider the modulo of Φ , i.e., as moving from 0 to 1, where 1 is, of course, equal again to 0.

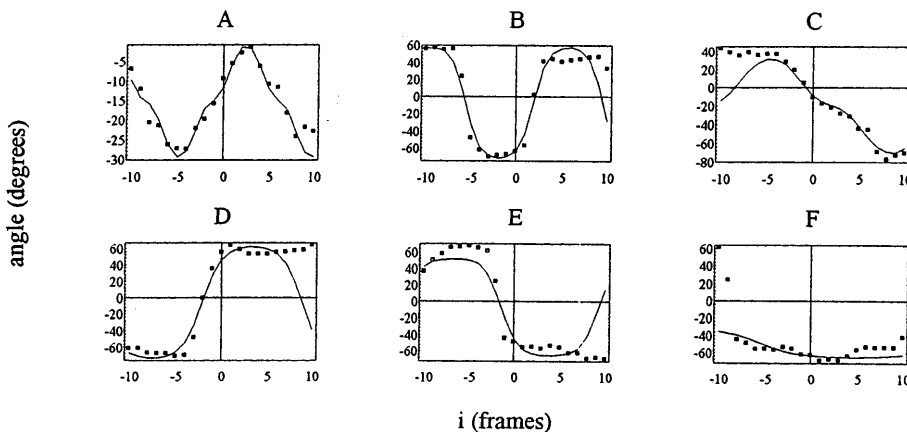


Fig. 4A–F. Six examples of “time windows” from the data (black dots), with the best fit curves generated by the Φ CAT algorithm (line). The data point around which the window was constructed is the one in the center ($i = 0$). The width of the windows is 21 frames = 0.84 s. The values obtained for the four parameters $\{C, A, T, \Phi\}$ of the curves in each window are, respectively, in units of {degrees, degrees, frames, cycles}: **A** $\{-15, 14, 15, 0.17\}$; **B** $\{-7, 65, 15, 0.38\}$; **C** $\{-19, 51, 26, 0.82\}$; **D** $\{-6, 68, 22, 0.15\}$; **E** $\{-7, 59, 21, 0.68\}$; **F** $\{-49, 16, 41, 0.62\}$

When the movement is more or less periodic, C , A , and T do not change much, while the phase descends regularly [it descends rather than ascends because the phase term in (1) appears with a minus sign instead of a plus; this arbitrary definition was chosen so that the phase would be truly analogous to the angle Φ in the phase-plane (Fig. 2, bottom), which turns clockwise]. If the movement of the segment is symmetrical relative to its next caudal segment, then $C = 0$. If the oscillation of the segment is asymmetrical, then $C \neq 0$. Intuitively, then, C represents the center around which the angle oscillates, and A represents the range of movement around this center. T represents the cycle period of the movement, e.g., the time interval between peaks.

When there is little or no movement, A approaches zero, and the entire term under the cosine in (1) and (3), including T and Φ consequently becomes meaningless. In graphical terms, when the amplitude of the time-series is very small, it becomes more difficult to measure the period and the phase (see, for example, Fig. 4F). In these situations, C equals the (unchanging) angle.

When the movement is not periodic but discrete, the ΦCAT algorithm models it as half a cycle of a periodic movement (see Fig. 4C, D). A typical discrete movement is ballistic; i.e., the angle first accelerates and then decelerates regularly. During this type of movement, A , C , and T do not change much, while the phase descends from 1 to 0.5 (if the segment moves to the right) or from 0.5 to 0 (if the segment moves to the left). As in periodic movement, C represents the center of movement (where angular velocity is the highest), A the movement's amplitude, and T its period (i.e., whether it was fast or slow). If, after the movement, the segment remains motionless, A vanishes, and T and Φ become meaningless again. The time window in Fig. 4E is centered around a frame in which the movement stops, and the amplitude starts to decline.

After the best-fit values of C , A , T , and Φ are obtained, the estimated angle y in the considered frame is given by (3) for $i = 0$. Figure 3 (top) shows the time series of the measured angle (represented by the dots), together with the estimated angle (solid line). It can be seen that, due to the partial overlapping of time windows centered on nearby frames, the algorithm produces

a good smoothing of the raw data. No other smoothing was used.

Both the widths of the time window and the weight function affect the results, and should therefore be chosen with care. We chose a large enough window so that the results were affected only by the weight function. A narrower weight function (higher weights to the center of the window relative to its edges) produced higher sensitivity to noise in the measurement of the angle, while a wider weight function reduces sensitivity to fast and short-term movements as well as to noise. An intermediate width should therefore be chosen, based on the frequency and noise of the measurement. We used a Gaussian with a standard deviation of three frames, so that movements shorter than about six frames (0.24 s) were smoothed and not considered.

3.3 Results of ϕ_{rel} computation

In order to see the wave of ϕ_{rel} , we used a visualization method we term a "phase raster" (Fig. 5). This can show the time series of both phase and amplitude of all the angles of the body at once. In the phase raster, each angle was assigned a horizontal row, in which the phase was coded by the circle of RGB colors: red for 0, green for 1/3, blue for 2/3, and red again for 1 = 0. The amplitude A was coded by the saturation of the color, from 0 (colorless) to 1 (saturated). The amplitude was normalized to units between 0 and 1 by dividing it by its range. Such visual coding is appropriate because phase (like color) is cyclic and has no meaning when the amplitude (saturation) is zero or very small.

The angles are ordered, from bottom upwards, in the order h, n, ff, c, p, hh , which is a cephalo-caudal order for the body angles. The foreleg angle ff is inserted after the neck angle n , and the hindleg angle hh is inserted after the pelvis angle p . The four last angles, ff, c, p, hh , are then repeated again, replicating the respective bottom rows. Such a representation shows traveling waves as diagonal stripes of the same color. An upward diagonal stripe indicates that the wave is cephalo-caudal. With this specific arrangement of the rows, the stripes pattern produced was continuous, and roughly two color cycles were present for each moment from bottom to top, in-

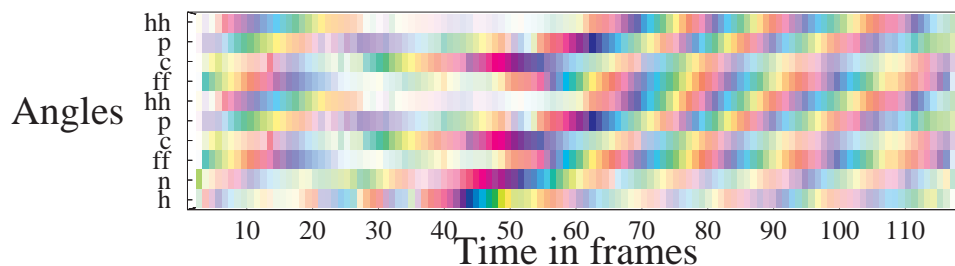


Fig. 5. A "phase raster" representing the free movement sequence shown in Fig. 2. The *horizontal axis* represents time (25 frames/s). Each of the six angles h, n, ff, c, p, hh is represented by a *horizontal row*. The phase is coded by the circle of RGB colors: red for phase 0, green for 1/3, blue for 2/3, and red again for phase 1 = 0. The amplitude A (normalized to units from 0 to 1 for each angle) is coded by the saturation of the color, going from colorless (no movement) to saturated (maximal amplitude of movement). The angles are ordered, from *bottom* to *top*, in a cephalo-caudal order, with the last four angles repeated again. See text for further explanation

dicating the tendency to a constant wavelength. Since two waves are simultaneously present with only four of the six angles repeated, this means that the length of the wave was a little less than one body length. Note that the slope of the stripes varies, indicating faster or slower waves, but the vertical distance between stripes of the same color tends to be similar, so that two stripes are vertically present.

The phase raster in Fig. 5 shows the same sequence described in Fig. 2. Frames 0–20 represent forward walking which has come to a stop, apparent as the dwindling of color in frames 20–50, especially in the foreleg (*ff*) and hindleg (*hh*) rows. The left bending of the head, neck and chest in frame 25 is seen as a small diagonal wave in blue to green to yellow, apparent in the rows of these angles, but lacking in the foreleg row (because this bend did not involve stepping). This wave continues in red to violet in frames 30–35 (with the head) and 40–45 (when it reaches the chest), indicating a movement to the right, back to a more or less straight posture. At about frame 35, a pronounced bend to the right (red to violet to blue) starts with the head and then travels caudally, as the animal makes a tight right turn. Note that the foreleg angle lags behind the chest, violating the regularity of the wave. This phenomenon was typical of turns that started from a stop: stepping with the forelegs was delayed, as they remained on the ground after the body had already turned. We also observed this phenomenon in rats, where it was especially evident during recovery from akinesia in lateral-hypothalamic rats (the straightjacket phenomenon, see Golani et al. 1979). The pronounced wave of the turn continues with green to yellow to red, which marks straightening and bending to the other side. Regular waves then continue until the end of the sequence, indicating forward walking.

As the phase Φ of each angle or “joint” can be computed in every frame, the ϕ_{rel} of any two angles α , β is simply their phase difference $\Phi_\alpha - \Phi_\beta$, taken as modulo 1 (i.e., ϕ_{rel} of -0.2 , for example, is the same as that of 0.8). The traveling wave pattern that was shown in the phase raster suggests that ϕ_{rel} of successive segments is stabilized to a specific value, as in the undulation swimming of fish. In other words, at each moment in time there is a similar difference between two adjacent rows on the phase raster. As explained in the introduction, the hypothesis of a cephalo-caudal traveling wave with a fixed wavelength is equivalent to the hypothesis that ϕ_{rel} between adjacent angles of the body is stabilized to a little less than one cycle (i.e., a slight delay of the more caudal angle). This hypothesis, which was illustrated in Fig. 5, is tested on the pooled data from all four animals in Fig. 6.

The first horizontal row in Fig. 6 shows conditional distributions of the ϕ_{rel} 's between adjacent angles, as a function of amplitude. The angle pairs between which ϕ_{rel} was computed are, from the left, head angle to neck angle, neck angle to chest angle, chest angle to pelvis angle, foreleg angle to neck angle, and hindleg angle to pelvis angle. The ϕ_{rel} (vertical axes), in units from 0 to 1, is replicated twice on each axis, i.e., the top half of each

graph is identical to its bottom half. This representation is used in order to highlight the continuity of ϕ_{rel} , since, like phase itself, it is cyclic (phase 1 = phase 0, and a short delay is the same as a long advance). A of each angle pair (horizontal axes) was defined as the sum of the angle amplitudes (for a justification, see below).

Conditional densities are presented as contour maps, with dark areas indicating high conditional densities and light areas indicating low ones. The conditional densities were computed by first partitioning the data into equal bins of A . This distribution is presented on the top of each graph. Each bin of A was then partitioned into sub-bins of ϕ_{rel} , and the number of points within each sub-bin was divided by the total number of points in that bin. The number of bins was chosen in each case as the maximal number that still produced a smooth conditional distribution. The range was chosen so that each bin included at least 100 points. The number of sub-bins was 10 (i.e., each sub-bin equals 0.1 cycles of ϕ_{rel}). Data are pooled from four animals; $n = 5797$ points (frames), which amount to 231 s and includes approximately 250 waves.

As expected, the left side of the distributions in the first row shows less significant preference for one value, since as the amplitude approaches zero, the phase (and consequently ϕ_{rel}) becomes meaningless. When the amplitude is considerable, however, there is a clear preference, in all angle pairs, for one which in all cases is smaller than 1 = 0 (in-phase) but clearly greater than 0.5 (anti-phase). Such a value corresponds to a short delay in the second angle in the pair, relative to the first. The preferred ϕ_{rel} is similar through the whole range of amplitudes that contained sufficient data to compute a significant distribution.

In small amplitudes, the preference for $\phi_{\text{rel}} = 0.5$ (anti-phase) is probably an artifact created by measurement errors of the markers' location, since such errors would always affect adjacent angles in an opposite way (increasing one angle and decreasing its neighbor).

The second row in Fig. 6 shows conditional distributions of the same pairs of angles for the same data, but this time as a function of the center of oscillation C . As with the amplitudes, the center of oscillation for each pair of angles is the sum of their C 's. The distributions clearly show that the preferred ϕ_{rel} changes little, if at all, when the movement is asymmetrical to one side (C distant from 0); i.e., bending and straightening are performed with the same ϕ_{rel} as in bending to one side and then bending to the other side.

Note that if, for example, the sum of C 's of the head and neck angles was 30° , this would mean that the sum of these angles, or the angle of the head relative to the chest, was 30° at the middle of the movement. At the peak of the movement, however, the angle of the head relative to the chest was 30° plus the sum of amplitudes of the head angle and neck angle. This is, of course, true only if both angles reach the middle or peak of their movement at the same time, i.e., $\phi_{\text{rel}} = 0 = 1$, while usually (as shown by the ϕ_{rel} distributions) it is smaller. This example, however, shows the rationale of adding the A 's and C 's of successive angles.

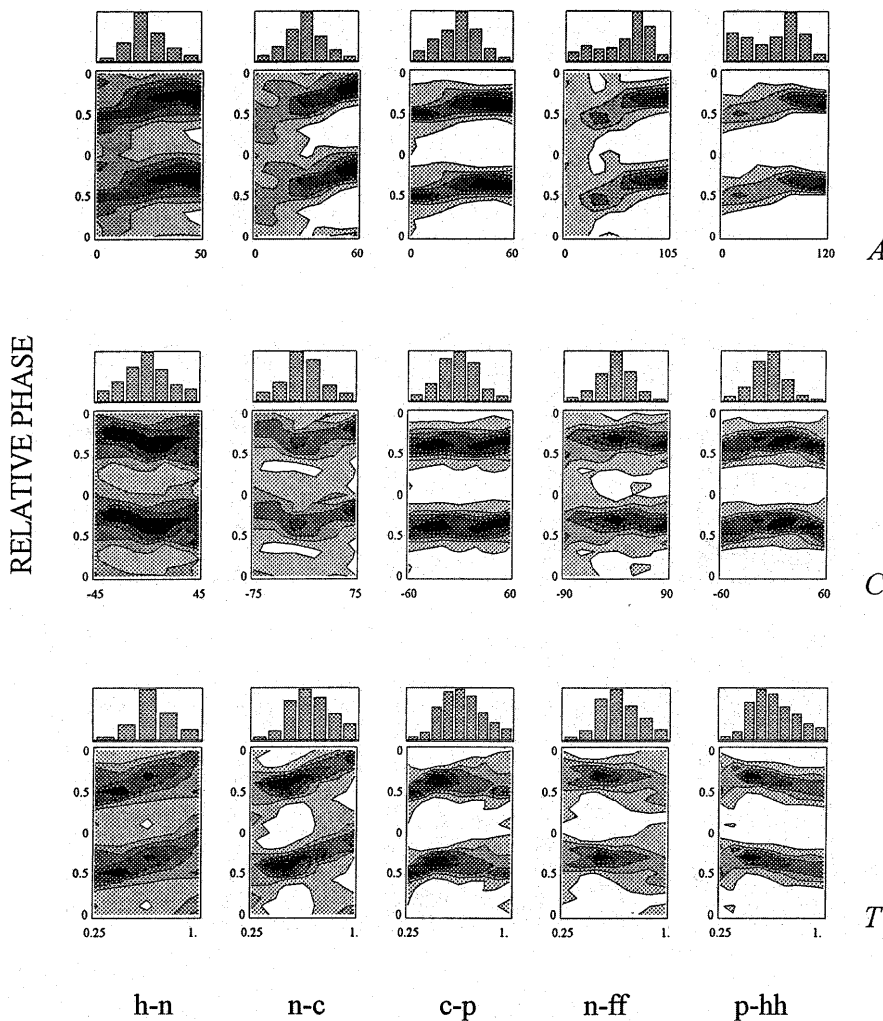


Fig. 6. Conditional distributions of ϕ_{rel} between adjacent angles, as a function of the amplitude A (first row), center of oscillation C (second row), and period T (third row). ϕ_{rel} is computed between head angle and neck angle (first column), neck angle and chest angle (second column), chest angle and pelvis angle (third column), neck angle and foreleg angle (fourth column), and pelvis angle and hindleg angle (fifth column). ϕ_{rel} (vertical axes) is in units from 0 to 1 = 0, and is replicated twice to show the continuity of the phase. For each pair of angles, the horizontal axis represents the sum of their amplitudes (first row), the sum of their centers of oscillation (second row), or the average of their periods (third row). Conditional densities are represented as contour maps, with dark areas indicating high conditional densities and light areas indicating low conditional densities. The conditional distributions were computed by first partitioning the data into bins of A (or C or T). This distribution is presented above each graph. Next, each bin was partitioned into sub-bins of ϕ_{rel} , and the number of data points within each sub-bin was divided by the total number of points within that bin. Data are pooled from four animals; $n = 5797$ points (frames), which amount to 231 s, comprising approximately 250 waves

The third row in Fig. 6 shows the conditional distributions of ϕ_{rel} for the same pairs of angles as a function of the period T . The period of every pair of angles was computed as the average of their periods. The range of T in which enough data points were available for a significant distribution was 0.25–1.0 s (7.5–25 frames). The distribution shows that, through an increase of T (which is the inverse of frequency) by the factor of 4, there is little change, if at all, in the preferred ϕ_{rel} . This result is similar to the situation in the undulation pattern of fish, where ϕ_{rel} does not change at different frequencies of undulation (Grillner and Kashin 1976; Grillner et al. 1995).

4 Discussion

The results of this work suggest that a considerable part of the ferret's free locomotor behavior (and, by implication, of both quadruped vertebrates and fish) may be understood as a generalization of the traveling wave in undulating fish. The generalization is suggested here in three different (albeit closely connected) directions:

1. In forward walking of quadruped vertebrates, the lateral movement of the body axis consists of a

traveling wave with a typical phase lag, as in the swimming of undulating fish;

2. Turning, in both quadrupeds and fish, consists of an asymmetrical wave, with a similar phase lag;
3. In quadrupeds, the movement of the legs in the horizontal plane while turning or walking can be considered as a part of this wave.

In the following, we will discuss each of these directions separately, and comment on some other implications of the results.

4.1 Traveling waves in forward locomotion of fish and tetrapoda

Fish of the archetypal body forms, i.e., anguilliform and carangiform, swim by means of lateral movements that travel from head to tail in a wavelike manner. This kinematic wave is due to a wave of muscle contractions traveling down along each side of the body. The wavelength of this traveling wave is stabilized to a fixed value of approximately one length of the body, across a wide range of swimming speeds and frequencies (Grillner and Kashin 1976). The exact value of the wavelength is determined by the fish form. In anguilliforms like the

eel and the lamprey, it is only about 2/3 of body length (i.e., there is more than one wave present at any time on the body), but in species in which the body form is shorter, the wavelength increases to one body length or even more (for a review, see Wardle et al. 1995). The fixed wavelength (within each species) implies that there is a constant ϕ_{rel} , or a cephalo-caudal “phase lag”, between successive segments of the body.

The lateral movement of the body in walking of tetrapoda is, in contrast, commonly thought of as involving a standing wave, as in a vibrating string or an elastic rod that is held at particular points (the “nodes” of the wave). In a standing wave, the nodes do not move laterally at all. Between any two adjacent nodes, the phase is the same (ϕ_{rel} between the segments is zero, so there is no phase lag or advance), while over a node the phase changes abruptly by half a cycle. In the phase raster in Fig. 5, a standing wave would appear as a chess pattern of the colors (rather than a diagonal pattern), horizontally divided at the nodes. The notion that walking in tetrapoda involves a standing wave is based on studies of the newt (Roos 1964), the salamander *Ambystoma tigrinum* (Frolich and Biewener 1992) and some lizards (Gans 1975; Avery et al. 1987). These studies led to the hypothesis that a major transition in the central pattern generators for locomotion occurred in the evolution of amniota (Bekkof 1985; Cohen 1988). We are not aware of any previous work that has investigated this question in mammals.

In other studies, however, it was found that terrestrial locomotion in other species of salamander (Edwards 1976, cited in Ritter 1992 and in Frolich and Biewener 1992) and lizards (Ritter 1992) involves a traveling wave, especially at high velocities of walking. Our finding shows that a traveling wave also coordinates lateral bending in the walking of a mammal. As shown in Fig. 5, the wavelength in the ferret is a little less than one body-length (from nose to tail), which is, interestingly, similar to that of the lamprey. Since walking is very different from swimming in biomechanical terms, this similarity among the vertebrates is perhaps due to a similar neural organization. Consequently, generalizing the neural basis for locomotion from the lamprey’s spinal cord may be more straightforward than it has seemed.

The evidence we present here for a traveling wave in a mammal may not be conclusive, perhaps, since we measured only five points along the body (excluding the tail) compared with the eight points of Ritter (1992) and 11 points of Frolich and Biewener (1992). Our method of computing and visualizing the results is preferable, however, because it can compute and show the phase lag between any two points on the body (Fig. 6) and all phase lags at once (Fig. 5). The two studies cited above measured the amount of lateral displacement (and in Ritter 1992 also the lateral velocity) of every point, looking for the nodes which reveal the existence of a standing wave. The nature of the wave was thus decided by only one or two points on the body, rather than by the pattern of all points. Further research is therefore needed to clarify whether quadruped vertebrates in

general and mammals in particular use a traveling wave, a standing wave, or both. In any case, analysis in terms of ϕ_{rel} and use of the Φ CAT algorithm and phase rasters shown here are likely to elucidate the pattern of lateral bending.

4.2 Turning as asymmetrical locomotion

Gray (1968) stated that in the turn of an anguilliform fish, “the amplitude of the wave of contraction which passes along the body on the side towards which the animal turns is greater than that on the other side of the body.” How exactly forward locomotion can be modulated into a turn is not clear from this statement. In particular, does the asymmetrical wave of turning also have a typical phase lag, and is it similar to the phase lag of the forward wave?

Turning in fish was investigated mainly in the context of a typical escape response, the C-start (e.g. Foreman and Eaton 1993), so-called because of the shape of the fish’s body as seen from above. This response provides an important experimental model for the reticular control of the spinal cord. Unfortunately, most studies on the C-start did not use anguilliform fish, in which the traveling wave is easy to measure, but fish with a short and stout body like the goldfish or sunfish (*Lepomis* sp.). Furthermore, the C-start is a very fast response, which means that resolution is poor not only in the phase dimension, but also in the time dimension. Most important, the phase was always measured by the traditional method of tracking points of maximum curvature along the fish axis. This method measures the length, in percentage of body-length, between points of maximum curvature (thereby actually measuring the inverse of the phase lag, i.e., body length per unit of phase difference, rather than the phase difference per unit of body length). This method is accurate and convenient with forward swimming, but not with turning. During a turn, the first wave of lateral bending can be seen by the point of maximum curvature, but the following wave of straightening cannot, since when the fish has a C-shape, this wave should be measured by the point of minimum curvature (instead of maximum curvature to the other side, as in forward swimming). Consequently, Jayne and Lauder (1993) were able to determine that at the time of the C-start, all kinematic events move posteriorly, but they did not measure the phase lag.

In contrast, in eel-like fish, the body is so elongated that it preserves the typical S-shape even during most of the turn, so that the phase lag can be determined by the traditional method. Ullen et al. (1993) investigated the response of river lampreys (*Lampreta fluviatilis* L.) to illumination, and also described their pattern of turning (Fig. 7, taken directly from Fig. 2A in Ullen et al. 1993). The points of maximum curvature are plotted in Fig. 8, which is recreated with additions from Fig. 2B in Ullen et al. (1993). As Ullen et al. reported, the turn (frames 0 to 15) included a “turning wave” that was slower than the normal undulatory wave of forward swimming (frames 15 to 18). What they did not state, however, is

that the vertical distance between the lines in Fig. 8 (plotted in bold lines, our addition) is the same during the turn and during the forward swimming. i.e., the phase lag is the same. Note also that during frames 9 to 12, the phase lag could not be computed because the lamprey assumed a true C-shape (Fig. 7), so that a point of maximum curvature existed only on one side. By using the Φ CAT algorithm, the phase lag during this time could have been determined as well.

It seems, therefore, that in both ferrets and lampreys, turning is generated with the same phase-lag as in forward walking. A thorough verification of this hypothesis is still necessary, however, for the lamprey. In both cases, a turn can be modeled by changing a single parameter, the center of oscillation C . It is interesting to note that the neural-mechanical model for lamprey swimming by Ekeberg (1993) also produces turning by asymmetric tonic stimulation, which causes an asymmetrical wave with a similar phase-lag (as can be judged from Fig. 6 in Ekeberg 1993). But although the turn seems similar to that of the real lamprey, to our knowledge this similarity has not been tested yet. Furthermore, since Ekeberg's model depends on the detailed neurophysiology and biomechanics of the lamprey, it cannot be applied directly to mammals or reptiles, nor, for that matter, to other fish.

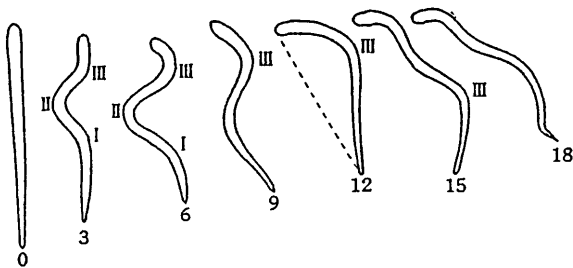


Fig. 7. A turn of a river lamprey (*Lampreta fluviatilis* L.), evoked by illumination of one side of the body. The illustration was taken from Fig. 2A in Ullen et al. (1993). Arabic numerals indicate frame numbers. Roman numerals indicate points of maximum curvature of the body. The "turning wave" is designated by III

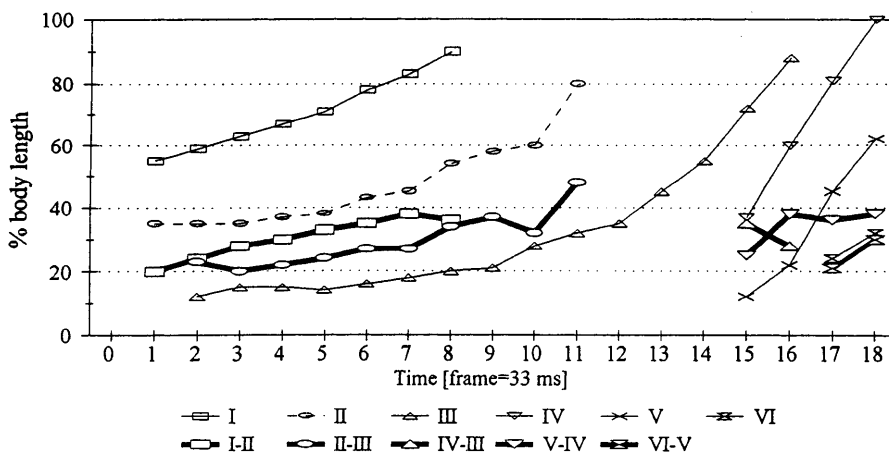


Fig. 8. The cephalo-caudal waves of curvature maxima during the turn shown in Fig. 7, recreated with additions from Fig. 2B in Ullen et al. (1993). *Thin lines* (waves) connect points of maximum curvature on the body. They are marked by the same Roman numerals as in Fig. 7. *Bold lines* indicate the distances, in percentage body-length, between any two adjacent waves (the vertical distance between adjacent thin lines)

4.3 Participation of the legs in the wave

In this study, we considered the two forelegs together as one "virtual" segment, and measured its ϕ_{rel} in reference to the chest. In a similar way, the hindlegs were considered as one virtual segment whose ϕ_{rel} was measured relative to the pelvis. This choice might seem arbitrary: would it not be preferable to consider each leg as a separate segment? And why not connect the ipsilateral or diagonal legs?

We chose not to consider each leg separately because, when turning from a standing position the ferret might start with a step backward with the inside (relative to the direction of turning) foreleg, or with a step forward with the outside foreleg, with no apparent preference. If the forelegs are considered as one segment connecting the paws, these two cases become equivalent. The same is true for the hindlegs. Considering the two forelegs together and the two hindlegs together enabled us to envisage their movement as part of the cephalo-caudal wave propagation in the phase raster, because if the movement includes only the anterior part of the body, the forelegs might step while the hindlegs remain anchored in place.

Clearly, the leg movement is far from being fully explained by the wave. By measuring only the (two-dimensional) location of the feet we ignored the vertical components of the leg movement. We also ignored the distance between the feet. The lateral component of stepping in vertebrates has been only partly investigated (Golani et al. 1979; Szechtman et al. 1985; Eilam and Golani 1988; Cools et al. 1989). Turning in ferrets (and in rats, see Szechtman et al. 1985; Kafkafi et al. 1996) may also change the diagonal order of stepping, e.g., eliminating the outside hindleg, and subsequently both hindlegs stepping as the turn becomes tight. These changes may be referred to as "subgaits", and the notion of phase transitions may be used to investigate them, as has been done with ordinary gaits (Schoner et al. 1990; Collins and Stewart 1993); e.g., the radius of the turn or some similar property may be shown to serve as a "control parameter" that induces bifurcations in the dynamics of stepping.

Although all these aspects were ignored in this study, our results nevertheless show the similarity between the legs and the parts of the body: both show the independence of ϕ_{rel} of C (and of A and T , but these results were expected, perhaps, for the legs; Fig. 6). This is consistent with the insight gained by the paradigm of coordination dynamics, according to which stable phase relationships are likely to arise in a complex system of coupled oscillators, regardless of the way the system variables are defined.

4.4 ϕ_{rel} dynamics and patterns of free behavior

The motivation behind this study was to establish a model of natural patterns of free behavior. In the behavioral neurosciences, it is still mostly impossible to define the basic units of free whole-animal behavior in an objective and autonomic way. By “objective” we mean that the definition and recognition of the pattern are formal and can be done without the subjective decision of an experienced observer, “as in judging a work of art” (Beer 1980). By “autonomic” we mean that the definition and recognition of the pattern can be accomplished solely on the basis of the morphology of behavior (i.e., movements and their coordination) and do not require outside considerations such as the assumed functions of the pattern, its mediating neural basis, or its evolutionary causes.

This problem of objective and autonomic definition of behavior patterns, especially in free behavior, has been avoided for a long time in all the disciplines of behavioral neuroscience, because of the patterns’ inherent complexity and their many degrees of freedom (for a discussion of this problem see Golani 1992; Golani and Kafkafi 1998). Recently, however, advances in the field of coordination dynamics suggested that this complexity may be explained by dynamical system models of coupled oscillators (e.g., Haken et al. 1985; Schoner et al. 1990; Turvey 1990; Yuasa and Ito 1990; Collins and Stewart 1993; Kelso 1995; Kafkafi et al. 1996). In most of these models, the ϕ_{rel} of concurrent movements (or some similar expression) is the key variable. This study shows that the ϕ_{rel} notion can be applied to free behavior. Based on its stability, it may be possible to construct dynamical models that reproduce, for example, the sequence of free movement shown in Fig. 2, with all its many degrees of freedom, using only a few variables and parameters.

This study could not have been done without developing the ΦCAT algorithm, which makes it possible to compute the ϕ_{rel} between any two movements, whether periodic or discrete. The modeling of every movement as a locally periodic movement may seem to be based on a far-fetched assumption. It is therefore important to stress that it is not meant here as a model for movement planning or execution in the motor system. It is only meant as the simplest model required for applying ϕ_{rel} measurements under free movement conditions. Nonetheless, treating discrete movements as half a limit cycle has been suggested by Schoner (1990, 1994) in his model for trajectory formation.

Several obstacles need to be overcome before a (two-dimensional) model for free locomotor behavior in the ferret can be constructed. This study demonstrates the statistical stability of ϕ_{rel} , which suggests that it might be a controlled variable. Its moment-to-moment dynamics, however, remains to be studied. This can be done by coordination dynamics methods such as return maps (see, e.g., Kelso 1995; Kafkafi et al. 1996). The effect of C , A , and T on ϕ_{rel} dynamics should be investigated. It is also possible that these or other parameters may induce bifurcations (phase transitions, see Haken et al. 1985) in ϕ_{rel} dynamics. Such bifurcations might explain, for example, a transition from a traveling to a standing wave pattern, should such a pattern be found.

In this study, each degree of freedom (i.e., every angle between the segments) was decomposed into four components, which might not seem to be moving in the direction of reducing the number of variables. Such decomposition is partially justified, however, because it shows that the phase components of all angles are closely related, thus assisting in reducing the actual number of degrees of freedom. It still remains to be examined whether the other components of each angle, A , C , and T , are also related across angles. Finally, all the variables in this study were defined in a body-related reference frame, while there is no doubt that variables in the absolute reference frame, e.g., the animal’s direction and speed, are also important. We are now investigating these questions.

Acknowledgements. We thank Dan Drai, Prof. Yoav Benjamini and Prof. Mark Shik for their comments on the manuscript. All experiments and actions comply with the current laws of the State of Israel. This research was supported by a grant from the Israel Academy of Sciences, Israel Science Foundation.

Appendix: technical considerations of implementing the ΦCAT algorithm

The ΦCAT algorithm is based on optimization of the parameters C , A , T , and Φ in (3) in order to yield the best fit to the data within the “time window” which is constructed around each data point. The optimization is done in such a way as to minimize the (weighted) sum of the squared differences between estimated and actual data (least-square optimization). The algorithm was implemented with the “NonlinearFit” function in the statistics package of Mathematica software (Wolfram Research Inc. 1993).

With this implementation the NonlinearFit function requires reasonable start values for C , A , T , and Φ , or it might lock on some unreasonably distant values which produce a local minimum of the sum of the squares. Such start values can easily be obtained by simple statistical methods. We found that in most cases the average of the data points in the considered time window yielded a good estimation of C , and their standard deviation yielded a good estimation of A . For these estimations, the size of the time window should be of the order of the typical period of cycles in the time series.

T and Φ can also be estimated by computing the angular velocity, or the first derivative of the time series (by subtracting each data point from its next neighbor). T is estimated by $2\pi/\omega$, where ω is the ratio between the standard deviation of the velocities and the standard deviation of the angles in the time window. Φ is estimated by:

$$\hat{\Phi} = \frac{1}{2\pi} \arctan \left[2\pi \frac{\alpha(i) - \hat{C}}{\hat{T}}, v(i) \right] \quad (4)$$

where \hat{C} and \hat{T} are the (previously computed) estimates for C and T in that window, $\alpha(i)$ and $v(i)$ are the angle and the angular velocity at the considered frame i (around which the time window is centered), and $\arctan(x,y)$ is the arc tangent of y/x , taking into consideration the quadrant in which the point (x,y) is located.

If the data have a high level of noise, it might be necessary to smooth the time series and the computed velocity. Smoothing, however, reduces the standard deviations of the angles and of the angular velocities in the time window, which are needed to estimate A and T . In this case, it may be necessary to increase the standard deviations by a certain factor in order to obtain good estimates. Additional improvements to the estimation process may be added, and their validity can be assessed by comparing the resulting cosine curve to the data.

In the very few cases in which the NonlinearFit function, starting from the above estimates, could not lock onto reasonable values, we chose the start value ourselves, by visually estimating the fit of the resulting cosine curve. Most of the time, however, these estimates were close enough to the final parameter values achieved by the best fit, so that the visualization and statistical analysis we describe in the results section yielded similar results with each. Since computing only the estimates is much faster than computing the best fit (by one to two orders of magnitude, depending on the window's width), it may be advisable to use only the estimates, especially when dealing with a large amount of data.

References

- Avery RA, Mueller CF, Smith JA, Bond J (1987) The movement of a lacertid lizard: speed, gait and pauses in *Lacerta vivipara*. *J Zool Lond* 211:47–63
- Beer CG (1980) Perspectives on animal behavior comparisons. In: Bornstein MH (ed) *Comparative methods in psychology*. Earlbaum, Hillsdale, NJ
- Bekkof A (1985) Development of locomotion in vertebrates: a comparative perspective. In: Gallin ES (ed) *Comparative development of adaptive skills: evolutionary implication*. Earlbaum, Hillsdale, NJ, pp 57–94
- Cohen AH (1988) Evolution of the vertebrate central pattern generator for locomotion. In: Cohen AH, Rossignol S, Grillner S (eds) *Neural control of rhythmic movements in vertebrates*. Wiley, New York, pp 129–166
- Collins JJ, Stewart IN (1993) Coupled nonlinear oscillators and the symmetries of animal gaits. *J Nonlinear Sci* 3:349–392
- Cools AR, Scheenen W, Eilam D, Golani I (1989) Evidence that apomorphine and α -amphetamine produce different types of circling in rats. *Behav Brain Res* 34:111–116
- Edwards JL (1976) A comparative study of locomotion in terrestrial salamanders. PhD dissertation, University of California at Berkeley
- Eilam D, Golani I (1988) The ontogeny of exploratory behavior in the house rat (*Rattus rattus*): the mobility gradient. *Dev Psychobiol* 21:679–710
- Ekeberg O (1993) A combined neuronal and mechanical model of fish swimming. *Biol Cybern* 69:363–374
- Foreman MB, Eaton RC (1993) The direction change concept for reticulospinal control of goldfish escape. *J Neurosci* 13:4101–4113
- Frolich LM, Biewener AA (1992) Kinematic and electromyographic analysis of the functional role of the body axis during terrestrial and aquatic locomotion in the salamander *Ambystoma tigrinum*. *J Exp Biol* 162:107–130
- Gans C (1975) Tetrapod limblessness: evolution and functional corollaries. *Am Zool* 15:455–467
- Golani I (1976) Homeostatic motor processes in mammalian interactions: a choreography of display. In: Bateson PPG, Klopfer PH (eds) *Perspectives in ethology*, Vol II. Plenum Press, New York, pp 69–134
- Golani I (1992) A mobility gradient in the organization of vertebrate movement: the perception of movement through symbolic language. *Behav Brain Res* 15:249–308
- Golani I, Kafkafi N (1998) The role of symbolic language and graphical visualization in understanding coordination patterns of free animal behavior. *Med J Israel*, special issue (in press)
- Golani I, Wolgin DL, Teitelbaum P (1979) A proposed natural geometry of recovery from akinesia in the lateral-hypothalamic rat. *Brain Res* 164:237–267
- Gray J (1933) Directional control of fish locomotion. *Proc R Soc Lond [Biol]* 113:115–125
- Gray J (1968) *Animal locomotion*. Weidenfeld and Nicholson, London
- Grillner S, Kashin S (1976) On the generation and performance of swimming in fish. In: Herman RM, Grillner S, Stein PSG, Stuart DG (eds) *Neural control of locomotion*. Plenum Press, New York, pp 181–202
- Grillner S, Deliagina T, Ekeberg O, El Manira A, Hill RH, Lansner A, Orlovsky GN, Wallen P (1995) Neural networks that coordinate locomotion and body orientation in lamprey. *Trends Neurosci* 18:270–279
- Haken H, Kelso JAS, Bunz H (1985) A theoretical model of phase transitions in human hand movements. *Biol Cybern* 51:347–356
- Jayne BC, Lauder GV (1993) Red and white muscle activity and kinematics of the escape response of the bluegill sunfish during swimming. *Comp Physiol A* 173:495–508
- Jung R, Kiemel T, Cohen AH (1996) Dynamic behavior of a neural network model of locomotor control in the lamprey. *J Neurophys* 75:1074–1086
- Kafkafi N, Levi-Havusha S, Golani I, Benjamini Y (1996) Coordination of side-to-side movements and walking in amphetamine treated rats: a stereotyped motor pattern as a stable equilibrium in a dynamical system. *Biol Cybern* 74:787–795
- Kelso JAS (1995) *Dynamic patterns*. MIT Press, Cambridge, Mass
- Kopell N (1988) Toward a theory of modeling central pattern generators. In: Cohen AH, Rossignol S, Grillner S (eds) *Neural control of rhythmic movements in vertebrates*. Wiley, New York, pp 129–166
- Rand RH, Cohen AH, Holmes PJ (1988) Systems of coupled oscillators as models of central pattern generators. In: Cohen AH, Rossignol S, Grillner S (eds) *Neural control of rhythmic movements in vertebrates*. Wiley, New York, pp 129–166
- Ritter D (1992) Lateral bending during lizard locomotion. *J Exp Biol* 173:1–10
- Roos PJ (1964) Lateral bending in newt locomotion. *Proc Ned Acad Wetten C* 67:223–232
- Schoner G (1990) A dynamic theory of coordination of discrete movement. *Biol Cybern* 63:257–270
- Schoner G (1994) From interlimb coordination to trajectory formation: common dynamical principles. In: Swinnen S, Heuer H, Massion J, Casaer P (eds) *Interlimb coordination: neural, dynamical and cognitive constraints*. Academic Press, San Diego, pp 339–368
- Schoner G, Jiang WY, Kelso JAS (1990) A synergetic theory of quadrupedal gaits and gait transitions. *J Theor Biol* 149:359–351
- Szechman H, Teitelbaum P, Ornstein K, Golani I (1985) The morphogenesis of apomorphine induced behavior in the laboratory rat. *Neurosci* 14:783–798
- Turvey MT (1990) Coordination. *Am Psychol* 45:938–953
- Ullen F, Orlovsky GN, Deliagina TG, Grillner S (1993) Role of dermal photoreceptors and lateral eyes in initiation and orientation of locomotion in lamprey. *Behav Brain Res* 15:107–110
- Wardle CS, Videler JJ, Altringham JD (1995) Tuning in to fish swimming waves: body form, swimming mode and muscle function. *J Exp Biol* 198:1629–1636
- Wolfram Research, Inc. (1993) Technical report – guide to standard Mathematica packages, Version 2.2, pp 396–399
- Yuasa H, Ito M (1990) Coordination of many oscillators in generation of locomotory pattern. *Biol Cybern* 63:177–184